MSH6- or PMS2-deficiency causes re-replication in DT40 B cells, but it has little effect on immunoglobulin gene conversion or on repair of AID-generated uracils

Campo, Vanina A ; Patenaude, Anne-Marie ; Kaden, Svenja ; Horb, Lori ; Firka, Daniel ; Jiricny, Josef ; Di Noia, Javier M

Abstract: The mammalian antibody repertoire is shaped by somatic hypermutation (SHM) and class switch recombination (CSR) of the immunoglobulin (Ig) loci of B lymphocytes. SHM and CSR are triggered by non-canonical, error-prone processing of G/U mismatches generated by activation-induced deaminase (AID). In birds, AID does not trigger SHM, but it triggers Ig gene conversion (GC), a 'homeologous' recombination process involving the Ig variable region and proximal pseudogenes. Because recombination fidelity is controlled by the mismatch repair (MMR) system, we investigated whether MMR affects GC in the chicken B cell line DT40. We show here that Msh6(-/-) and Pms2(-/-) DT40 cells display cell cycle defects, including genomic re-replication. However, although IgV GC tracts in MMR-deficient cells were slightly longer than in normal cells, Ig GC frequency, donor choice or the number of mutations per sequence remained unaltered. The finding that the avian MMR system, unlike that of mammals, does not seem to contribute towards the processing of G/U mismatches in vitro could explain why MMR is unable to initiate Ig GC in this species, despite initiating SHM and CSR in mammalian cells. Moreover, as MMR does not counteract or govern Ig GC, we report a rare example of 'homeologous' recombination insensitive to MMR.

DOI: https://doi.org/10.1093/nar/gks1470

3032–3046 *Nucleic Acids Research, 2013, Vol. 41, No. 5* *Published online 11 January 2013*
doi:10.1093/nar/gks1470

MSH6- or PMS2-deficiency causes re-replication in DT40 B cells, but it has little effect on immunoglobulin gene conversion or on repair of AID-generated uracils

Vanina A. Campo[1,2,3], Anne-Marie Patenaude[1], Svenja Kaden[4], Lori Horb[1], Daniel Firka[5], Josef Jiricny[4] and Javier M. Di Noia[1,2,3,6,*]

[1]Institut de Recherches Cliniques de Montréal, Division of Immunity and Viral Infections, Montréal, H2W 1R7 Québec, Canada, [2]Department of Microbiology and Immunology, Université de Montréal, Montréal, H3T 1J4 Québec, Canada, [3]Department of Medicine, Université de Montréal, Montréal, H3T 1J4 Québec, Canada, [4]Institute of Molecular Cancer Research of the University of Zurich and the ETH Zurich, 8057 Zurich, Switzerland, [5]Druida Software and Consulting, M5R 1X5 Toronto, Ontario, Canada and [6]Division of Experimental Medicine, Department of Medicine, McGill University, Montréal, H3A 1A3 Québec, Canada

Received September 25, 2012; Revised December 17, 2012; Accepted December 18, 2012

ABSTRACT

The mammalian antibody repertoire is shaped by somatic hypermutation (SHM) and class switch recombination (CSR) of the immunoglobulin (*Ig*) loci of B lymphocytes. SHM and CSR are triggered by non-canonical, error-prone processing of G/U mismatches generated by activation-induced deaminase (AID). In birds, AID does not trigger SHM, but it triggers *Ig* gene conversion (GC), a 'homeologous' recombination process involving the *Ig* variable region and proximal pseudogenes. Because recombination fidelity is controlled by the mismatch repair (MMR) system, we investigated whether MMR affects GC in the chicken B cell line DT40. We show here that *Msh6*$^{-/-}$ and *Pms2*$^{-/-}$ DT40 cells display cell cycle defects, including genomic re-replication. However, although *IgVλ* GC tracts in MMR-deficient cells were slightly longer than in normal cells, *Ig* GC frequency, donor choice or the number of mutations per sequence remained unaltered. The finding that the avian MMR system, unlike that of mammals, does not seem to contribute towards the processing of G/U mismatches *in vitro* could explain why MMR is unable to initiate *Ig* GC in this species, despite initiating SHM and CSR in mammalian cells. Moreover, as MMR does not counteract or govern *Ig* GC, we report a rare example of 'homeologous' recombination insensitive to MMR.

INTRODUCTION

The antibody repertoire of higher organisms is firstly generated by VDJ recombination, followed by additional genetic modification through somatic hypermutation (SHM), immunoglobulin gene conversion (*Ig* GC) and class switch recombination (CSR). During SHM, nucleotide changes are introduced into the exons encoding the variable (*IgV*), N-terminal domain of the antibody heavy and light chains by a mechanism involving error-prone DNA polymerases [reviewed in (1,2)]. Although *Ig* GC serves the same purpose, mutations are not introduced directly but are copied from numerous pseudogene sequences located upstream on the same chromosome (3,4). In contrast, CSR involves the fusion of the *IgV* to a different constant (effector) region by double-strand break-induced region-specific recombination [reviewed in (5,6)].

SHM, *Ig* GC and CSR are all initiated by activation-induced deaminase (AID) (7–9), an enzyme expressed in antigen-stimulated B cells, which typically converts multiple cytosines in the *Ig* loci into uracils (2).

*To whom correspondence should be addressed. Tel: +1 514 987 5642; Fax: +1 514 987 5528; Email: javier.di.noia@ircm.qc.ca
Present addresses:
Vanina A. Campo, IIB-INTECH, San Martin, Buenos Aires, Argentina.
Lori Horb, Marine Biological Laboratory, Bell Center for Regenerative Biology and Tissue Engineering, Woods Hole, MA, USA.

Although uracil is generally highly efficiently repaired by base excision repair (BER), this process seems to be inefficient in antigen-stimulated B cells. Thus, some uracils persist until the next round of replication to give rise to C:G to T:A transition mutations (1,2). Others are removed by uracil–DNA glycosylase (UNG) (10–12), but the resulting abasic sites persist and are bypassed by translesion polymerases to yield all types of mutations at C:G base pairs (2,13). A third group of uracils is addressed by a poorly defined pathway, which involves MutSα (11,14), a heterodimer of mutS homologue 2 (MSH2) and MSH6 that normally initiates DNA mismatch repair (MMR) (15,16). It was proposed that MutSα detects G/U mismatches generated by AID and triggers an error-prone, long-patch repair process that introduces mutations at sites distal to those deaminated by AID (1,2). A related mechanism that involves MutSα and other factors was postulated to act at *Ig* switch regions to give rise to double-strand breaks that trigger CSR in the absence of UNG (11,17). The molecular mechanism of MMR-mediated diversification of *Ig* genes remains to be elucidated, but genetic experiments implicated exonuclease I (18), DNA polymerase η (19,20) and monoubiquitylated proliferating cell nuclear antigen (21,22) in this process. Interestingly, MutLα, a heterodimer of mutL homologue 1/postmeiotic segregation increased S cerevisiae 2 that acts immediately downstream of MutSα during MMR (15), plays no role in SHM [reviewed in (1)], although it can influence the chromosome rejoining pathway during CSR (23). The roles of UNG and MutSα in mammalian antibody diversification seem to be partially redundant, given that only their combined deficiency abrogates both CSR and SHM. Thus, in $Ung^{-/-}$ $Msh2^{-/-}$ or $Ung^{-/-}$ $Msh6^{-/-}$ mice, *Ig* lesions are limited to C:G to T:A transitions (11,24).

That antibody diversification can also involve *Ig* GC was first shown in chickens (3,4), and probably contributes to antibody diversification in most bird species (25) and rabbits (26), and perhaps in other species (25). The *IgV* exons, *VJ* in the light chain and *VDJ* in the heavy chain, are located downstream from an array of *V*, *VJ* and *VDJ* pseudogenes (referred to as ψV) that serve as donors in the gene conversion reactions. *Ig* GC replaces a contiguous stretch of 8 to >200 nucleotides and can thus introduce multiple base changes into the recipient *V(D)J* sequence (27), which may translate into amino acid replacements affecting the specificity and/or affinity of the antibody.

The chicken DT40 B cell lymphoma line undergoes constitutive AID-dependent *Ig* GC (28,29), and it is widely used to study antibody diversification (25,30,31) as well as DNA repair (31–33). *Ig* GC in DT40 cells is commonly used as a model for homologous recombination (HR) repair because the initiating event is well defined and requires HR factors, including the RAD51 paralogues XRCC2, XRCC3 and RAD51B (34), BRCA1 (35), BRCA2 (36) and RAD54 (37).

Unexpectedly, MMR does not seem to initiate *Ig* GC in DT40 cells, given that UNG inhibition or knockout largely eliminated Ig GC, accumulating instead C to T mutations (38,39). This implies that, unlike the mammalian enzyme (11,24), chicken MutSα does not recognize AID-generated G/U mismatches, that MMR-dependent processing of G/U mispairs does not take place in this system in the absence of UNG or that MMR-mediated processing of G/U mispairs in DT40 cells is mostly error-free, as seen in a proportion of AID-generated uracils in mouse B cells (40). However, even if MMR does not trigger *Ig* GC, it would be still predicted to affect its outcome; it should restrict it by preventing recombination between sequences that are too diverged (41–45), while, on the other hand, helping to repair mismatches arising through annealing of non-identical (homeologous) donor and recipient DNA sequences (31,33,46,47). Although MSH6-, MSH4- or MSH3-deficient cells were reported to undergo *Ig* GC [previously mentioned (7) as data not shown], the role of MMR in this process has not been studied in detail or compared with HR.

In this study, we describe the effect of MutSα and MutLα deficiency on the frequency, fidelity and overall quality of *Ig* GC in DT40 cells. Our data reveal that MMR is largely dispensable in this process, possibly because of its limited contribution towards processing of AID-generated uracils at the *Ig* locus. Moreover, we find that *Ig* GC represents a rare case of 'homeologous' recombination that is insensitive to the anti-recombination effects of MMR.

MATERIALS AND METHODS

Cell lines and transfections

DT40 IgM^- CL18 (28) or its IgM^+ derivative CL18c4 (34) was grown in 5% CO_2 at 41°C in RPMI 1640 with glutamine (Wisent) supplemented with 10% FCS (Wisent), 1% chicken serum (Invitrogen), 50 μM β-MSH and antibiotics. DT40 $Aid^{-/-}$ was a kind gift of Dr H. Arakawa and Dr J.M. Buerstedde (7). Transfections for gene targeting and MSH6 complementation were as previously described (10,34). Retroviral particles for DT40 transduction were produced in HEK293T cells co-transfected with a plasmid for VSV-G, a plasmid for MLV gag/pol and the retroviral vector pMIG or pMIG-Ugi. HEK293T supernatant was harvested 48 h post-transfection, filtered and added to 10^6 DT40 cells in the presence of 8 μg/ml of polybrene in 24-well plates.

Gene targeting

The structure of the chicken *Msh6* and *Pms2* genes was determined by assembling the sequence of multiple polymerase chain reaction (PCR) products amplified from DT40 genomic DNA using oligonucleotides designed to span one or more introns based on the gene structure of the murine genes. The oligonucleotide sequences were based on the corresponding chicken cDNAs assembled from multiple expression sequence tags obtained from GeneBank™. The structures of the genes, targeting and screening strategies were confirmed by Southern blot. The targeting constructs were assembled in pBluescript II (Supplementary Figure S1). Antibiotic resistance cassettes were described earlier (48). The *Msh6* targeting construct

eliminates the last 20 amino acids encoded by exon 4 and most of the 3′-adjacent intron, including the splice donor site, and creates a frameshift. The *Pms2* targeting construct eliminates exons 7 and 8 of the gene. Genomic DNA was purified using Puregene DNA isolation kit (Gentra) and digested with BamHI–EcoRI for screening *Msh6* targeting or BamHI–XbaI for *Pms2*. Probes were labelled by PCR using 2 μM dATP/dAGT/dTTP and 50 μCi of [α-^{32}P]dCTP and oligonucleotides OV1 (TGG GAGCAGGTAGTTTTGTG) and OV2 (CTCTGGGAT GTCAGCAAGTC) for *Msh6* and OJ43 (TGACAGGTT CTGCGTTCATA) and OJ44 (TAGGGCAGCATTCCA TTC) for *Pms2*. Probes were purified using Illustra MicroSpin G-50 columns (GE Healthcare), and filters were hybridized in ExpressHyb (Clontech) and developed by PhosphorImager (GE Heathcare).

Growth and cell cycle analysis

Growth curves were generated by diluting exponentially growing cultures to 5–10 × 10^5 cells/ml that were kept in the log phase by appropriate dilutions. Trypan blue-excluded cells were periodically counted in a haemocytometer and corrected for dilution factor. Population doubling times were calculated from exponential curve fits of cell numbers versus time plots using Prism 5 (GraphPad software Inc). Cloning efficiency was estimated by fluorescence-activated cell sorting (FACS)-depositing single cells into 150 μl of normal culture medium in 96-well plates and counting the number of viable clones per plate after 2 weeks. DNA content profiles were determined by flow cytometry of 2 × 10^6 cells fixed in cold 70% ethanol, and stained in 0.5% Triton X-100, 100 mg/ml of RNase A and 60 mg/ml propidium iodide. S-phase profiles were determined by flow cytometry in cells pulsed for 30 min at 37°C in medium containing 10 μM BrdU (Sigma). Cells were fixed as described earlier in the text, and DNA was denatured in 2 N HCl 0.5% Triton X100, neutralized with 1 M $Na_2B_4O_7$ pH 8.5 and labelled with anti-BrdU-fluorescein isothiocyanate (FITC) antibody (BD Biosciences) and propidium iodide. Apoptosis was determined by Annexin V-FITC staining (Sigma). Drug sensitivity was measured by culturing 50 000 cells for 24 h in 96-well plates in increasing concentrations of 6-thioguanine (Sigma). Viability was estimated by MTS reduction using Celltiter 96® Aqueous non-radioactive cell proliferation assay (Promega).

Antibody diversification assays

For IgM phenotype fluctuation analysis, homogeneous IgM^+ or IgM^- populations were obtained by FACS after blocking for 10 min in phosphate-buffered saline, 1% bovine serum albumin, 3% normal goat serum and staining for 30 min with anti-chicken IgM-FITC (Bethyl, 1:200). Dead cells were excluded by propidium iodide staining (10 μg/ml). Multiple 500 000 cell populations were cultured in 24-well plates for a given number of population doubling times, splitting 1:2 every 1 or 2 days, and their surface IgM phenotype determined by flow cytometry. Where indicated, the culture medium was supplemented with 1.25 nM Trichostatin A (TSA) (Sigma). Cells expressing Ugi or the control retrovirus were selected by GFP expression and stained using anti-chicken IgM-PE mAb (Southern biotech). Reduced UNG activity was confirmed by enzymatic assays as described previously (10).

Sequence analysis

IgM^+ or IgM^- cells (1–5 × 10^5) from the expanded DT40 populations were sorted by FACS, resuspended in DirectPCR (Viagen) and extracted with proteinase K. The variable region of the rearranged DT40 λ light chain locus was PCR amplified using KOD DNA polymerase (Novagen) [95°C 2 min + 8 × (95°C 20 s, touch down 68 >60°C 10 s, 70°C 1 min) + 23 × (95°C 15 s, 60°C 10 s, 70°C 1 min) + 72°C 5 min]. PCR products were A-tailed, cloned into pGEM-T-Easy (Promega) and sequenced by Macrogen Inc (Seoul, Korea) using the SP6 oligonucleotide. Sequences were aligned using Sequencher (Genecodes). Mutations were scored and assigned to all possible donor pseudogenes using Mutdet, a tailor-made software (D.F. and J.M.D.N., unpublished data) that assigned all possible gene conversion events following described criteria (10,34,38). Mutdet results were then manually verified. The pseudogene that could explain the most consecutive mutations and had the longest homology encompassing all mutations was scored as the donor. The maximum gene conversion tract was defined as the longest sequence fragment sharing perfect homology between each IgVλ sequence analysed and the pseudogene explaining the most consecutive mutations.

MMR and gel-shift assays

DT40 cell extracts were prepared by lysing the cells in isotonic lysis buffer [10 mM Tris–HCl, pH 7.5, 2 mM $MgCl_2$, 3 mM $CaCl_2$, 0.32 M sucrose, 1 mM dithiothreitol, 0.1 mM spermine, 0.5 mM spermidine, 0.3% IGEPAL CA-630 and complete inhibitor cocktail (Roche)]. For gel-shift assays, 10 μg of the respective DT40 cell extracts was incubated with 40 fmol of [^{32}P]-labelled G/T, G/C or +1 duplexes (generated, respectively, by annealing the oligonucleotides CCA GAC GTC TGT **T**GA CGT TGG GAA GCT TGA G, CCA GAC GTC TGT **C**GA CGT TGG GAA GCT TGA G or CCA GAC GTC TGT C**T**G ACG TTG GGA AGC TTG A to CTC AAG CTT CCC AAC GTC **G**AC AGA CGT CTG G or CCA GAC GTC TGT CAA **U**GT TGG GAA GCT TGA G to CTC AAG CTT CCC AAC GTT GAC AGA CGT CTG G, all written 5′–3′) in 25 mM HEPES–KOH, pH 8.0, 0.5 mM ethylenediaminetetraacetic acid, 10% (v/v) glycerol, 0.5 mM dithiothreitol and 1 μg of Poly[d(I:C) – d(I:C)] for 20 min at room temperature in a final volume of 20 μl. Samples were separated on 5 or 6% TAE–polyacrylamide gels. The dried gels were exposed to a PhosphorImager screens.

A detailed procedure for the MMR assays has been described previously (49). Briefly, heteroduplex DNA substrates containing a G/T mismatch or a one nucleotide insertion (+1) within a SalI restriction site, or a G/U mispair within an AclI restriction site in the 46-bp

polylinker of a pGEM13Zf(+) derivative, were constructed by primer extension, using the mismatch-containing 31mer oligonucleotides 5′-CCA GAC GTC TGT **T**GA CGT TGG GAA GCT TGA G-3′ for the G/T mismatch substrate, 5′-CCA GAC GTC TGT C**T**G ACG TTG GGA AGC TTG A-3′ for the +1 substrate or 5′CCA GAC GTC TGT CAA **U**GT TGG GAA GCT TGA G-3′ for the G/U substrate (the mispaired or inserted residue is highlighted in bold) and the single-stranded phagemid DNA as template. The strand discrimination signal was introduced by incubation with N.BstNBI, which introduced a specific nick into the complementary strand (3′ from the mismatch) at position 350 of the duplex. Isolation of the desired supercoiled heteroduplex substrates and the MMR assays were carried out as described, using 100 ng (47.5 fmol) heteroduplex DNA substrate and 80 μg of DT40 cell extracts in a volume of 25 μl. After 45 min of incubation at 37°C, the reactions were terminated by adding 10 μg of proteinase K and heat inactivation at 55°C for 2 h. After purification of the DNA on a Qiagen MinElute Reaction Cleanup Kit, samples were digested with SalI and DraI or AclI, respectively, treated with 10 μg of RNaseA overnight and then run on a 1% TAE–agarose gel containing 0.5 × Gel-Red (Biotium). To inhibit BER in assays using the G/U substrate, Thymine DNA glycosylase (TDG) was immunodepleted as previously described (49), and the extracts were pretreated for 10 min with 4U of Ugi (NEB) at 37°C to inhibit UNG.

Statistics

Statistical analysis was performed using Prism 5 (GraphPad software Inc).

RESULTS

Growth defects in MSH6- and PMS2-deficient DT40 cells

We targeted the MMR pathway in DT40 cells by disrupting either the *Msh6* or *Pms2* genes (Supplementary Figure S1). Loss of MSH6 selectively depletes MutSα, which plays an important role in both SHM and CSR, but not MutSβ, which is not involved in SHM or CSR (50–52), but which might affect other recombinogenic events. Similarly, loss of PMS2 depletes MutLα, which plays a role in CSR [reviewed in (1,2,5)], but it should not affect the other MLH1-containing heterodimer MutLγ (MLH1/MLH3), which participates in recombination (53). The chicken MSH6 and PMS2 proteins have not been characterized but share high similarity in primary sequence as well as in their structural and functional features with their mouse and human orthologues (Supplementary Figure S2).

To our surprise, $Msh6^{-/-}$ and $Pms2^{-/-}$ DT40 cells displayed major growth defects. Both cell lines had considerably longer lag phases (not shown) and a ∼2-fold increase in the population doubling times during exponential growth (Figure 1A and B). In addition, their cloning efficiencies were extremely low (Figure 1C). Because such drastic growth phenotypes have not been described in MMR-deficient cells from other organisms, we wanted to verify that they were indeed a consequence of the MMR deficiency. We, therefore, complemented the DT40 $Msh6^{-/-}$ line with human MSH6. This largely rescued growth and cloning efficiency (Figure 1A–C), which suggests that the phenotype is indeed caused by the MMR gene defect. The difference between wild type (WT) and hMSH6-complemented $Msh6^{-/-}$ cells could be caused by sequence divergence between chicken and human MSH6 (Supplementary Figure S2) and/or insufficient expression levels of the complemented cells. The heterozygous $Msh6^{+/-}$ and $Pms2^{+/-}$ cells displayed only small increases in population doubling times, but both showed reduced cloning efficiency, albeit to a much lesser extent than the homozygous knockouts (Figure 1B and C). It seemed conceivable that the observed growth defects were related to DNA damage caused by AID. However, as doubly deficient $Msh6^{-/-}$ $Aid^{-/-}$ DT40 cells had similar growth defects to $Msh6^{-/-}$ cells (Figure 1D), this was not the case. Ablation of MSH6 or PMS2 in a second, IgM^{+}, DT40 line CL18c4 led to similar phenotypes and showed an IgM^{dull} subpopulation, which was constant over time and likely, another manifestation of the growth defects (Figure 1E). We, therefore, conclude that normal DT40 growth is dependent on the MMR pathway.

Cell cycle alterations in MSH6- and PMS2-deficient DT40

Unlike parental DT40, logarithmically growing $Msh6^{-/-}$ and $Pms2^{-/-}$ cells showed many Trypan blue-positive cells indicative of necrotic cell death (data not shown). Although we observed a trend towards higher spontaneous apoptosis in the $Msh6^{-/-}$ and $Pms2^{-/-}$ cells (Figure 2A), this was too small to account for the growth defects. Microscopic examination showed morphologically abnormalities in the $Msh6^{-/-}$ and $Pms2^{-/-}$ cultures, with numerous cells larger than normal. These cells had larger, often bi- or multilobular nuclei (Figure 2B), which suggested cell cycle checkpoint defects. Indeed, analysis of DNA content confirmed cell cycle alterations, with reduced proportion of cells in S-phase and a significant number of cells with >4n DNA content (Figure 2C). Complementation of $Msh6^{-/-}$ DT40 cells with hMSH6 corrected these defects to a large extent (Figure 2C). 2D cell cycle analysis of $Msh6^{-/-}$ cells using BrdU incorporation to distinguish cells in S-phase revealed a defect in DNA damage-induced G_2/S checkpoint (Figure 2D), as previously described for MMR-deficient cells (54). More importantly, a second cycle of replication and a distinct cell population with 8n DNA content were visible in $Msh6^{-/-}$ cells, indicative of endore-duplication (Figure 2D). Thus, MMR-deficiency in DT40 causes cell cycle defects and re-replication that are most likely responsible for the impaired growth.

MMR deficiency does not increase *Ig* gene conversion frequency

We analysed the frequency of *Ig* GC to test whether MMR counteracted this process, either through error-free

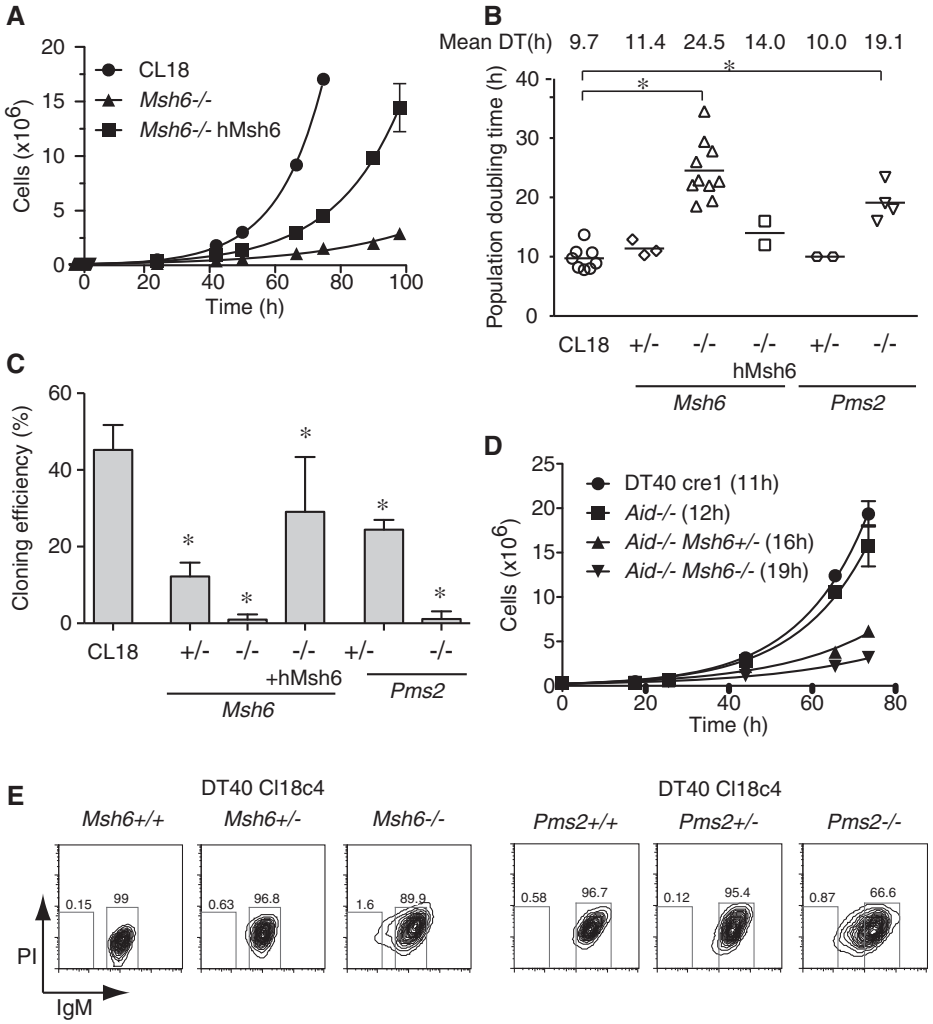

Figure 1. Impaired proliferation in MMR-deficient DT40 cells. **(A)** Growth curves of log-phase cultures of DT40 CL18 cells, its *Msh6*$^{-/-}$ derivative 1015 and the latter clone expressing human Msh6 (hMsh6). Average cell numbers, corrected by dilution factor, of duplicate cultures ± standard error of the mean are plotted over time. **(B)** Population doubling times were calculated by exponential curve fit ($R^2 \geq 0.95$ in every case) of growth curves as in (A). Multiple measurements for both DT40 parental lines used in this work (CL18 and CL18c4) are plotted, as well as one or more measurements of at least two independent cell lines for each of the indicated genotypes. Mean population doubling times (DT) are indicated at the top. **(C)** Cloning efficiency determined as the proportion of clones arising per 96-well plate after single cell deposition. Mean + standard deviation (SD) of —six to nine plates from two to three experiments are plotted. **(D)** Growth curves as in (A) with DT indicated in brackets next to each cell line. **(E)** Flow cytometry profiles of the IgM$^+$ DT40 cell line CL18c4 (*Msh6*$^{+/+}$ and *Pms2*$^{+/+}$ panels) along with representative *Msh6*$^{+/-}$ and *Msh6*$^{-/-}$ or *Pms2*$^{+/-}$ and *Pms2*$^{-/-}$ derivatives. In (B) an (C), $*P < 0.05$ ANOVA with Bonferroni's post-test.

repair of G/U mispairs or through its anti-recombination activity. The frequency of *Ig* GC can be estimated from fluctuation analysis of the surface IgM phenotype in DT40 (Figure 3A) (34). In brief, multiple subclones of the IgM$^-$ DT40 CL18 cell line, which has a frameshift in *IgV*λ preventing IgM expression (28), are expanded over time. Reversion of the frameshift by constitutive *Ig* GC allows re-expression of IgM with the median proportion of IgM$^+$ cells in the clonal populations providing an estimation of *Ig* GC frequency. As the proportion of IgM$^+$ cells increases with clonal expansion time, any difference in growth kinetics would affect these assays, which was a major concern in this case. Moreover, we could not obtain *Msh6*$^{-/-}$ or *Pms2*$^{-/-}$ single-cell clones (Figure 1C). We, therefore, modified the fluctuation assay by setting up multiple populations at exponential growth density ($\sim 0.5 \times 10^6$ sIgM$^-$ cells/ml). These large starting populations bypassed the defect in cloning efficiency and minimized the distorting effects that the much longer lag phase in more diluted *Msh6*$^{-/-}$ and *Pms2*$^{-/-}$ cultures would have on *Ig* GC frequency. To account for the different growth rates, we expanded the cell populations for the same number of generations, which were calculated from the respective population doubling times. We confirmed that the median proportion of IgM$^+$ cells increased linearly with the number of population doublings for DT40 WT as well as *Msh6*$^{-/-}$ cells (Figure 3B and C). When we used this method to compare the DT40 CL18 to multiple independent *Msh6*$^{-/-}$ or *Pms2*$^{-/-}$ derivatives, we observed interclonal variability. Nevertheless, although the median proportion of IgM$^+$ cells arising from DT40 *Msh6*$^{-/-}$ was reduced for one

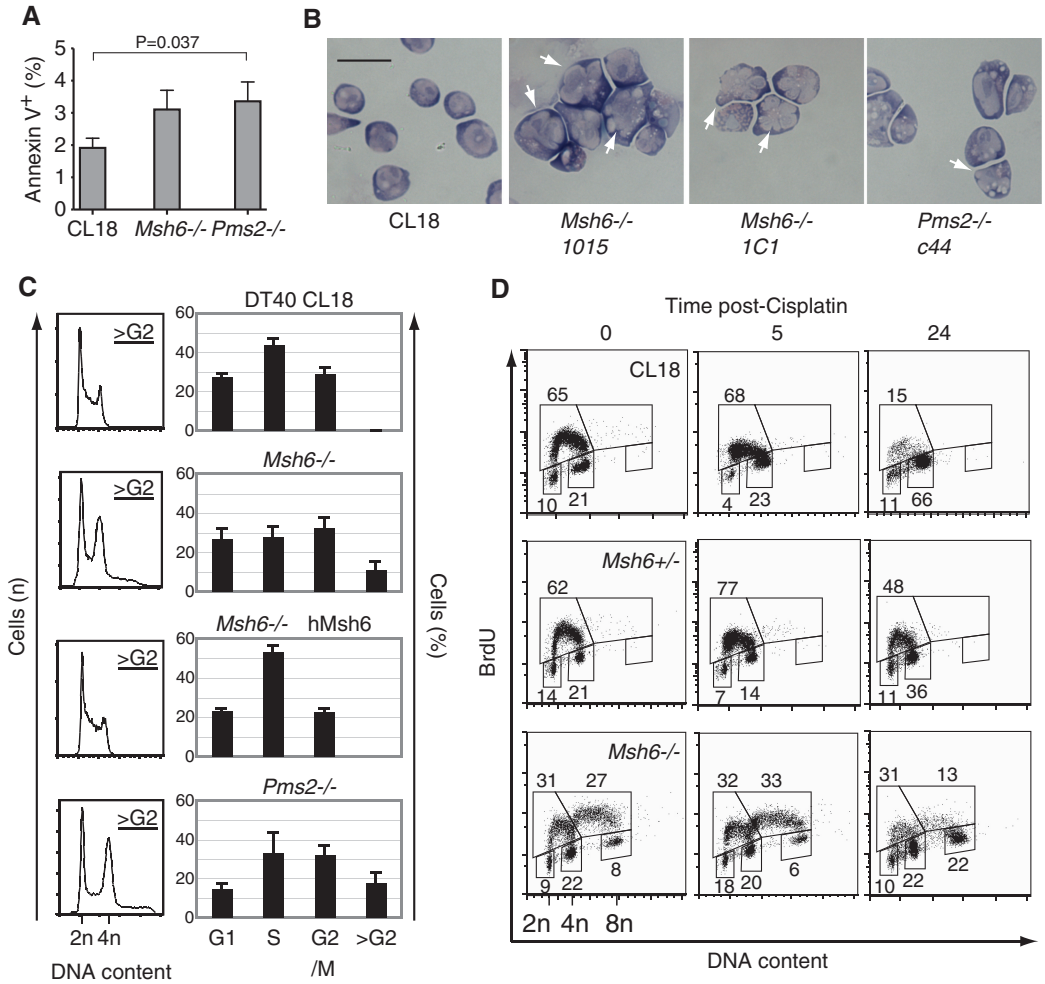

Figure 2. Cell cycle defects in MMR-deficient DT40 cells. **(A)** Proportion of AnnexinV-positive cells in exponentially growing cultures of the indicated DT40 cell lines. Mean + SD of —five to seven measurements done on CL18 and two independently derived knockout cell lines are plotted. Statistical significance by Student's unpaired two-tailed *t*-test. **(B)** Representative H&E staining images illustrating the presence of large cells with abnormal nuclear morphology in MSH6- and PMS2-deficient DT40. Bar, 20 µm. **(C)** Cell cycle profile of exponentially growing populations of DT40 cells. DNA was stained with propidium iodide and analysed by flow cytometry. 2n and 4n indicate the G_1 and G_2/M peaks, respectively (left panels). The population of cells with DNA content >4n was defined as $>G_2$. The bar graphs summarize the mean + SD proportion of cells in each cell cycle stage obtained from seven replicates for CL18 and *Msh6*$^{-/-}$, two replicates for *Msh6*$^{-/-}$ hMsh6 and three replicates for *Pms2*$^{-/-}$ (right panels). **(D)** 2D cell cycle analysis of DT40 cells pulsed with BrdU at 0, 5 or 24 h post-cisplatin treatment. BrdU incorporation into DNA was probed with FITC-labelled anti-BrdU antibody and DNA content by propidium iodide staining by flow cytometry. The proportion of cells in each gate is indicated. One representative of two experiments performed is shown.

line, it was not significantly different in three others (Figure 3D). Similarly, one DT40 *Pms2*$^{-/-}$ line generated only few IgM$^+$ cells, but two others were significantly different neither from CL18 nor from their *Pms2*$^{+/-}$ parental lines. The variability in IgM$^+$ proportion between lines could not be accounted for by variations in AID levels (Figure 3E; data not shown) nor did it correlate with their relative population doubling times. We suspect these variations to be because of different compensatory adaptations arising in the MMR-deficient lines during clonal expansion and growth. Importantly, *Ig* GC in *Msh6*$^{-/-}$ cells proceeded through its canonical mechanism. First, UNG deficiency caused by expressing the protein inhibitor Ugi in two independent DT40 *Msh6*$^{-/-}$ cell lines inhibited *Ig* GC as shown by a decrease in the frequency of IgM$^+$ cells (Figure 3F) (38). Second, analysis of DT40 *Msh6*$^{-/-}$ *Aid*$^{-/-}$ lines showed that ablation of *Msh6*$^{-/-}$ did not result in spontaneous *Ig* GC in the absence of the initiating lesion even on treatment with Trichostatin A (Figure 3G), which exacerbates *Ig* GC in DT40 cells (55).

The frequency of *Ig* GC could be overestimated when normalized to population doubling times, which is influenced by cell death. Nevertheless, the BrdU pulse-chase experiments suggest that the cell cycle is longer in MMR-deficient than in WT DT40 cells given the persistence of a higher proportion of BrdU$^+$ cells in *Msh6*$^{-/-}$ and *Msh6*$^{+/-}$ cells 24 h post-pulse (Figure 2D; data not shown). In any case, when logarithmically growing cells were expanded for the same length of time, *Ig* GC was still apparent, although its frequency in MMR-deficient DT40 cells was ~2- to 4-fold lower than in the control population

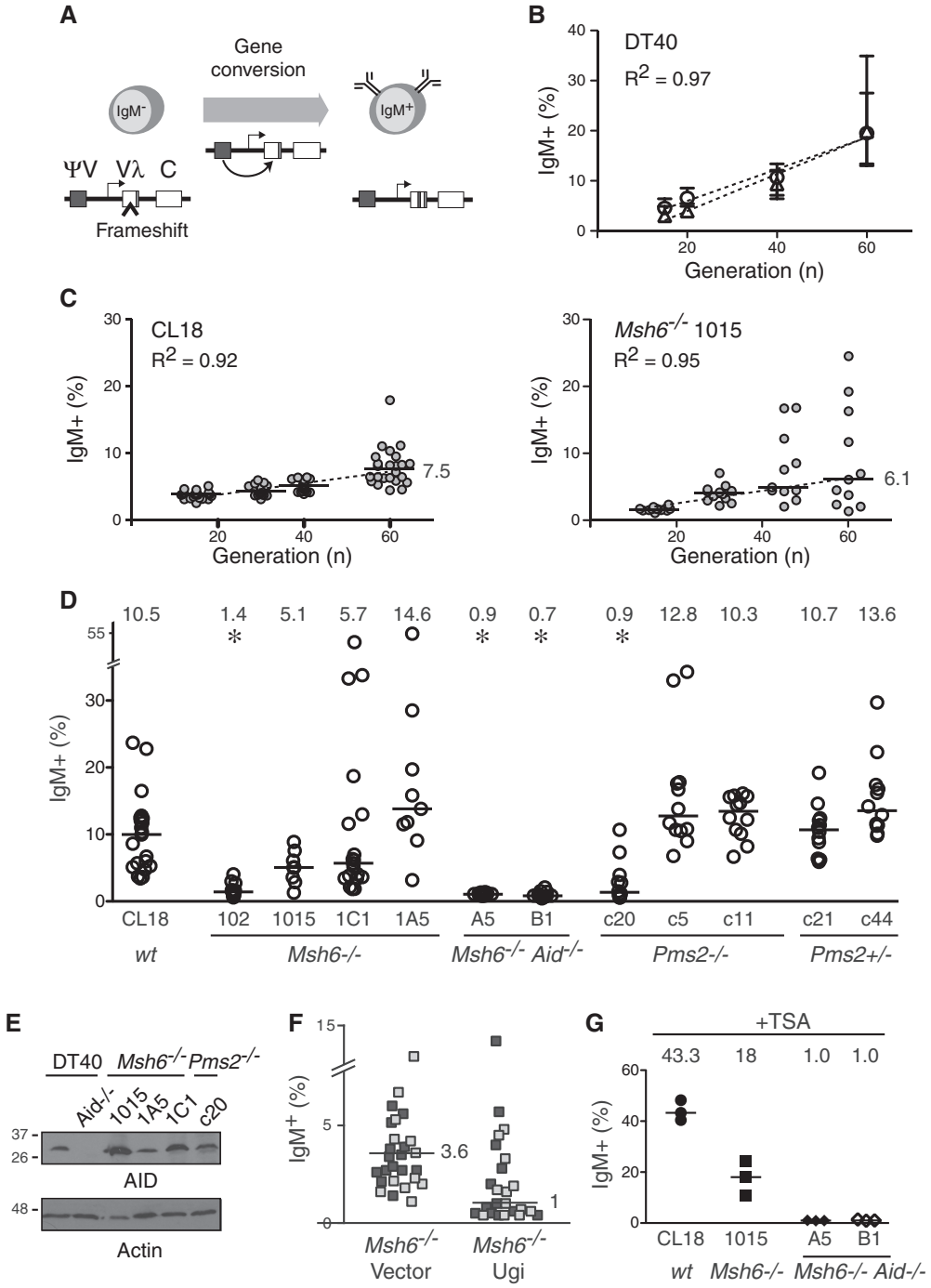

Figure 3. No increase in *Ig* GC frequency in $Msh6^{-/-}$ or $Pms2^{-/-}$ DT40 cells. **(A)** Scheme of the frameshift reversion assay used to estimate *IgVλ* gene conversion frequency by measuring the proportion of DT40 cells gaining surface IgM expression over time. **(B)** Linear correlation between median proportion of IgM-gain cells and generation number (defined by population doubling time) for multiple DT40 CL18 subpopulations kept in exponential growth. The proportion of IgM^+ cells arising from 24 subpopulations of IgM^- cells was determined by flow cytometry at each indicated number of generations. Median values and data range for two independent experiments (circles and triangles) are plotted with linear fit shown. **(C)** Multiple IgM^- subpopulations of DT40 CL18 ($n = 24$) and its $Msh6^{-/-}$ derivative line 1015 ($n = 12$) were sorted, independently expanded and analysed for IgM-gain as in (B) after 15, 30, 45 and 60 generations. The IgM^+ proportion values are indicated for each subpopulation with medians plotted as horizontal bars. Linear fit of the medians is shown. **(D)** IgM-gain in multiple subpopulations of CL18 ($n = 19$), its $Msh6^{-/-}$ derivative lines 102 ($n = 12$), 1015 ($n = 9$), 1C1 ($n = 19$) and 1A5 ($n = 9$), $Msh6^{-/-}$ $Aid^{-/-}$ A5 ($n = 12$) and B1 ($n = 12$), $Pms2^{-/-}$ lines c20 ($n = 20$), c5 ($n = 12$) and c11 ($n = 12$) and the $Pms2^{+/-}$ c21 ($n = 12$) and c44 ($n = 12$) (parentals to $Pms2^{-/-}$ c5 and c11) after 70 generations was determined as in (C). The proportion of IgM^+ cells in each subpopulation is plotted with medians indicated by horizontal lines and the value above. $^*P < 0.05$ Kruskal–Walis non-parametric test with post-test. **(E)** Total lysates of DT40 cell lines were separated by sodium dodecyl sulphate–polyacrylamide gel electrophoresis, and AID and actin levels were analysed by western blotting. **(F)** Populations of 50 IgM^- CL18 $Msh6^{-/-}$ cells expressing or not Ugi were sorted into 96-well plates and expanded for 45 generations. The proportion of IgM^+ cells is plotted for each population (two shades of grey distinguish independent $Msh6^{-/-}$ lines) with median values indicated. **(G)** Three IgM^- subpopulations of DT40 CL18, $Msh6^{-/-}$ line 1015 or $Aid^{-/-}$ $Msh6^{-/-}$ lines A5 and B1 were expanded for 45 generations in the presence of 1.25 nM TSA. The proportion of IgM^+ cells in each subpopulation is plotted with median values indicated.

(e.g. compare *Ig* GC for CL18 at 60 generations to *Msh6*$^{-/-}$ 1015 at 30 generations in Figure 2C; data not shown).

We conclude that MSH6 and PMS2 are dispensable for *Ig* GC, and that their deficiency does not result in any obvious change in *Ig* GC mechanism (i.e dependence on AID and UNG). We cannot formally rule our that MSH6 and PMS2 might be required for optimal *Ig* GC (see later in the text), but our results show that their absence does not lead to an increase in *Ig* GC frequency.

MMR deficiency does not significantly affect the outcome *Ig* gene conversion

As the growth defects in MMR-deficient DT40 cells hinder accurate calculation of Ig GC frequency, we analysed the GC events by sequencing the *IgVλ* region amplified from IgM$^+$ cells. This analysis provides information about multiple parameters that could be affected by MMR (Supplementary Figure S3), can be unequivocally scored and are less influenced by cell growth. Thus, we analysed the GC donor pseudogene usage, GC tract length, number of GC events per sequence and frequency of untemplated point mutations. We compared independent (not clonally related) *Ig* GC events obtained from multiple subpopulations of various DT40 lines grown for the same number of generations.

Ig GC in chickens prefers using the most similar pseudogene as donor (27). The pseudogene ψV*L8* is most closely related in sequence to DT40 *Vλ* (~90% overall, ~97% around the frameshift insertion) (Supplementary Figure S4), and, as anticipated, it was most frequently used to correct the frameshift in DT40 CL18 (Figure 4A). This preference was retained in the *Msh6*$^{-/-}$ or *Pms2*$^{-/-}$ cells (Figure 4A). We observed slightly longer GC tracts in DT40 *Msh6*$^{-/-}$ cells than in CL18, but this difference was not significant, irrespective of whether the data from each independent *Msh6*$^{-/-}$ line were analysed separately or pooled (Figure 4B and C). A clearer trend towards longer *Ig* GC tract lengths in the *Pms2*$^{-/-}$ cells became statistically significant when the analysis was restricted to *Ig* GC events templated on ψVL8 (Figure 4C). This eliminates confounding effects, such as differences in the length, relative orientation or degree of homology of different pseudogenes with the *IgVλ*.

We then compared the number of mutagenic events per sequence. Should MMR-deficient cells be more permissive for recombination, one would expect more GC events per sequence. However, this was not the case (Figure 4D). Alternatively, if MutSα was recognizing AID-generated G/U mispairs to initiate faithful MMR, *Msh6*$^{-/-}$ cells would be expected to display more single base pair mutations at the *IgV*. This was also not the case. The data set of sequences obtained from IgM$^+$ cells arising from IgM$^-$ populations had a similar ratio of point mutations per mutated sequence in CL18 and *Msh6*$^{-/-}$ or *Pms2*$^{-/-}$ lines (Figure 4E). A complementary experiment analysing mutations in the *IgV* of IgM-loss cells originating from the IgM$^+$ *Msh6*$^{-/-}$ did not show any increase in mutations either (Table 1). Combining MSH6 deficiency with UNG inhibition by expressing Ugi in two independent CL18c4 *Msh6*$^{-/-}$ lines increased untemplated point mutation frequencies (Table 1), but not beyond what others and us have observed in UNG-deficient DT40 cells (38,39). Thus, MSH6 or PMS2 deficiency seems to lead to a small increase in the length of the GC tracts, but does not affect the donor preference or the number of mutagenic events per sequence at the *IgVλ* locus of DT40 cells during *Ig* GC.

MMR in DT40 cells is functional, and homologous recombination is heterology sensitive

The lack of effect of MMR-deficiency on *Ig* GC or mutation frequency was striking. We, therefore, asked whether MMR was active in DT40 cells. We measured their sensitivity to 6-thioguanine (6-TG), which, once incorporated into DNA and methylated, generates mismatches with C that cause futile MMR cycles, DNA fragmentation and cytotoxicity (56). As anticipated, WT DT40 cells were sensitive to 6-TG, whereas *Msh6*$^{-/-}$ cells were resistant (Figure 5A). *Pms2*$^{-/-}$ cells were also more resistant to 6-TG than WT cells, albeit to a lesser extent than *Msh6*$^{-/-}$ cells (Figure 5A). Together with the biochemical evidence described later in the text, these results show that MMR is active in DT40 cells. Despite this, DT40 cells fail to reject *Ig* GC intermediates, which must have heterologies. We, therefore, set out to test whether HR in DT40 cells might generally tolerate heterology, especially given that one of the key hallmarks of DT40 cells is their high efficiency of targeted integration (57) mediated by HR (32). To this end, we used gene targeting as an assay. The *Msh6* disruption construct inactivated the first *Msh6* allele with 35% efficiency. We generated a modified version of this construct containing 15 mutations within the 1764-bp-long 5′-arm (Figure 5B). This represents only 0.8% of heterology, well below the ~10% divergence between *Ig VL* and the donor pseudogenes (3); yet, it was sufficient to completely abolish targeting (Figure 5C and D). Because of their negligible cloning efficiency, we were unable to formally demonstrate that gene targeting sensitivity to heterology in DT40 *Msh6*$^{-/-}$ and *Pms2*$^{-/-}$ cells is MMR-dependent. However, this has been well demonstrated in bacteria (58), yeast (59) and mammalian cells (44,60,61). Thus, our findings show that MMR is functional in DT40 cells, and that these cells tightly control the fidelity of HR *in vivo*, most likely through MMR.

Extracts of DT40 cells process G/U mispairs efficiently but predominantly by BER

To unequivocally demonstrate that MMR is biochemically active in DT40 cells and in an attempt to identify the possible cause(s) of the lack of effect of MutSα and MutLα loss on GC, we examined the substrate specificity of avian MMR. We first carried out gel-shift experiments with DT40 extracts. As shown in Figure 6A, mismatch-specific complexes were formed on incubation of the WT extracts with oligonucleotide heteroduplexes containing a G/T mispair or one extrahelical nucleotide (+1). The homoduplex G/C formed only unspecific complexes in these extracts (lane 1) (62). The fact that only the unspecific complexes were observed in extracts

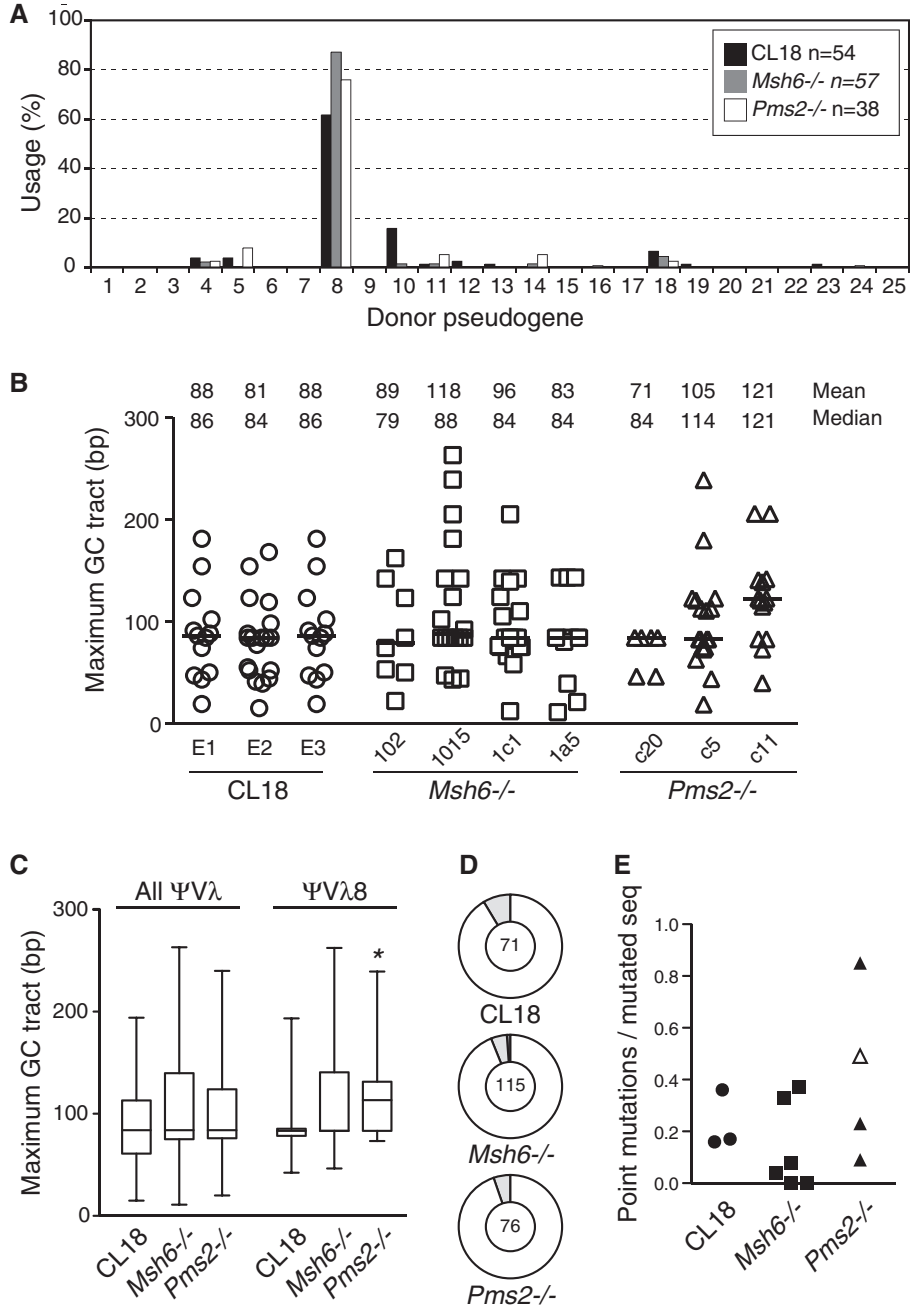

Figure 4. Unaffected *Ig* gene conversion fidelity in *Msh6*$^{-/-}$ and *Pms2*$^{-/-}$DT40. **(A)** Donor pseudogene usage. Proportion of *IgVλ* conversion events templated on each of the 25 *IgV* pseudogenes plotted for DT40 CL18, *Msh6*$^{-/-}$ and *Pms2*$^{-/-}$. The data compile sequences from subpopulations coming from several fluctuation experiments (CL18 $n = 3$, *Msh6*$^{-/-}$ $n = 6$ and four independent lines, *Pms*$^{-/-}$ $n = 3$ and three independent lines). The distribution was not significantly different between the different genotypes (two-way ANOVA). **(B)** Maximum gene conversion tract length was determined for each event obtained from CL18 (three independent experiments, E1–E3) as well as from independent lines of *Msh6*$^{-/-}$ (two fluctuations compiled for lines 1015 and 1C1) or *Pms2*$^{-/-}$. Tract length for each event is plotted with the mean and median (horizontal bars) values above. Differences are not significant by Kruskal–Walies non-parametric test. **(C)** All data from (B) were aggregated by genotype in box plots with 25–75% percentiles divided by the median and whiskers representing the minimum and maximum values. On the right, a similar plot considered only conversion tracts templated on pseudogene VL8. *$P < 0.05$ Kruskal–Walis non-parametric test with post-test. In (A–C), only independent events were considered (i.e. identical events found in sequences coming from the same subpopulation were excluded to prevent counting dynastically related events more than once). **(D)** The number of sequences containing one (white), two (grey) or three (black) conversion events were plotted as proportion of all sequences containing gene conversion events (n, indicated in the central circle). **(E)** The ratio of point mutations per mutated sequence was calculated for multiple data sets. The highest value in the *Pms2*$^{-/-}$ data set is biased by the presence of four sequences with multiple clonally related mutations. The empty triangle is the value for the same data set after removing these sequences. Clonally related sequences were not excluded in (D) and (E).

Table 1. Mutations in CL18c4-derived *Msh6*$^{-/-}$ DT40 cells sorted for IgM-loss

		Msh6$^{+/+}$	*Msh6*$^{-/-}$			
	Clone	CL18c4	c414		c429	
	Population analysed	IgM^{-}	IgM^{low}	IgM^{low} Ugi[a]	IgM^{low}	IgM^{low} Ugi
Sequences	n	83	69	24	72	24
	Mutated n (%)	39 (47)	10 (14)	12 (50)	3 (4)	14 (58)
Gene conversions	Independent[b]	15	6	2	0	1
	Total	15	6	3	0	1
	Per mut seq[c]	0.38	0.6	0.25	-	0.1
Point mutations	Independent[c]	15	3	10	1	14
	Total	16	4	12	1	15
	Per mut seq[c]	0.4	0.4	1	0.3	1.1
	Ambiguous[d]	8	4	2	2	2
Insertion/deletions		8	0	0	0	0

[a]The endogenous UNG activity was inhibited *in vivo* during expansion of the populations by expressing the Ugi protein.
[b]Identical events within a population were excluded to avoid recounting dynastically related events.
[c]All, rather than independent, events were considered to calculate mutation load per mutated sequence.
[d]Single base pair substitutions that could have been templated or untemplated.

of the *Msh6*$^{-/-}$ cells (lanes 2, 3, 5, 6, 8, 9) confirmed that the cells lacked MutSα. Moreover, this result showed that MutSβ in DT40 cell extracts either does not bind the +1 substrate or is present in undetectable amounts. We failed to detect specific complexes with the G/U substrate even on supplementation of the extracts with Ugi. This implied either that, unlike the human protein (63), avian MutSα does not recognize this substrate, or that the uracil was removed from the oligonucleotide substrate by a glycosylase other than UNG. *Pms2*$^{-/-}$ extracts contained similar levels of MutSα to WT extracts (Supplementary Figure S5). To confirm that the binding affinity was reflected in repair efficiency, we carried out *in vitro* MMR assays using DT40 cell extracts and a phagemid heteroduplex containing a G/T mispair in a SalI restriction site, which makes it refractory to cleavage with this enzyme. The phagemid also contained a nick as a strand discrimination signal 3′ from the mispaired T. In this scenario, both MutSα and MutLα are absolutely required for successful MMR. Digestion of the unrepaired phagemid with DraI and SalI gives rise to fragments of 2484 and 694 bp. On correction of the G/T mismatch to G/C, the SalI site is restored, such that the 2484 fragment is cut into fragments of 1324 and1160 bp. Repair efficiency can thus be estimated from the ratio of the 2484 and 1324 (or 1160) fragments. As shown in Figure 6B, ~30% of the G/T substrate was repaired in DT40 WT extracts (lane 2). In contrast, extracts of *Pms2*$^{-/-}$ (lane 3) and *Msh6*$^{-/-}$ (lane 5) cells were repair deficient. The lack of activity was not caused by poor quality of the extracts, given that MMR could be restored by the addition of recombinant human MutLα or MutSα, respectively (lanes 4 and 6). Importantly, although the WT extracts addressed the +1 substrate with similar efficiency to G/T (Figure 6C, compare lanes 2 and 4), we failed to detect repair of either substrate in extracts of *Msh6*$^{-/-}$ cells (lane 5), unless they were supplemented with recombinant MutSα (lane 6). This confirms the results of the gel-shift experiments and implies that MutSβ in DT40 extracts is either absent, or that it does not address an insertion/deletion loop of one extrahelical nucleotide, an intermediate arising during *Ig* GC, the processing of which is required to convert IgM^{-} cells to IgM^{+} phenotype.

We also wanted to learn how the extracts processed a G/U mispair. As shown in Figure 6D (lanes 2–6), this substrate was quantitatively converted to G/C in all three extracts. The repair efficiency was diminished on TDG depletion and Ugi addition (lanes 7–11), but supplementation with recombinant MutSα or MutLα failed to increase it, which implied that MMR does not contribute to the processing of G/U mispairs in our assay, and that these mispairs are addressed almost exclusively—and efficiently—by BER. Intriguingly, the limited effect of Ugi addition and TDG depletion suggested that the extracts contain another efficient uracil DNA glycosylase. It could be TDG because we cannot estimate efficiency of its immunodepletion by the anti-human TDG antibody other than from the additive effect of UNG inhibition by Ugi and TDG immunodepletion on the *in vitro* MMR assay (Supplementary Figure S6), but we cannot exclude the presence of another enzyme, such as MBD4 (64), given that DT40 cells lack SMUG1 (65).

DISCUSSION

The near absence of *Ig* GC in UNG-deficient DT40 cells implied that MMR does not activate an alternative pathway of uracil processing for initiating *Ig* GC (10,39). This was unexpected, given that MMR compensates to a substantial extent for UNG-deficiency for SHM and CSR (11,24). Moreover, *Ig* GC is a process of homeologous recombination, which is believed to involve MMR in at least two stages (Supplementary Figure S2). To gain insights into the criteria that govern *Ig* GC, we disrupted the *Msh6* or *Pms2* genes in DT40 cells. In this way, we selectively inactivated two key MMR complexes,

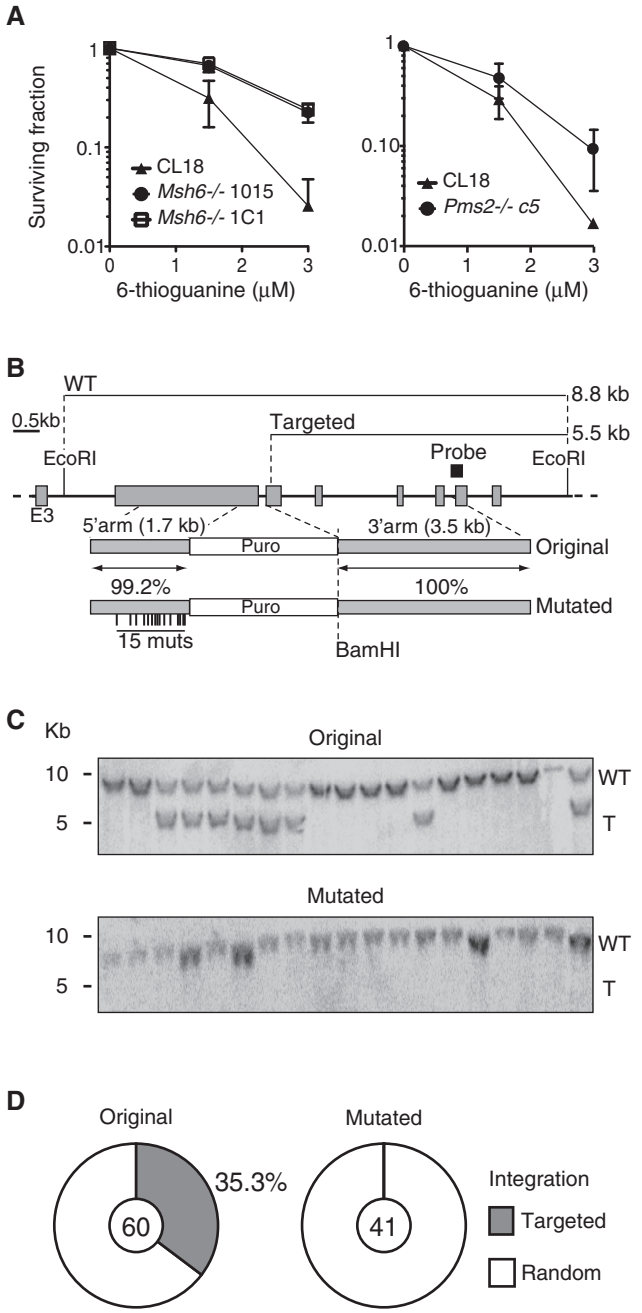

Figure 5. Mismatch sensing and heterology sensitive homologous recombination to in DT40. **(A)** Two independent *Msh6*$^{-/-}$ (left panel) and one *Pms2*$^{-/-}$ (right panel) lines and their respective parental DT40 cells were treated with increasing doses of 6-TG, and surviving fraction was determined 48 h later by MTS viability assays. Mean + SD of three experiments are plotted. **(B)** Partial scheme of chicken *Msh6* and the fully homologous and mutated targeting constructs. The position of the mutations and homology between the constructs are indicated under each relevant segment. The restriction enzymes and probe used for Southern blot, as well as the expected fragment sizes, are shown. **(C)** Representative Southern blots of DNA from puromycin-resistant clones digested with EcoRI and BamHI. The position of DNA size markers (left), as well as the wild-type (WT) and targeted (T) fragments, are indicated. **(D)** Proportion of clones having targeted (grey) and random (white) integration of the homologous or mutated *Msh6* constructs. The pie charts compile results from two independent experiments with the total number of clones analysed for each construct indicated in the centre.

MutSα and MutLα, respectively, which have been clearly implicated in mammalian antibody diversification (14,23,52,66,67). At the same time, the knockouts do not affect the other MSH and MLH heterodimers (MutSβ and MutLγ), which have no role in these processes (50–52).

MMR and DT40 cell viability

MMR has not been studied in avian cells to date. The sequence and structure of MSH6 and PMS2 are conserved between chicken and their mammalian counterparts (Supplementary Figure S2), and our results show that MMR in DT40 cells is functionally similar to MMR in other species (it confers sensitivity to 6-TG, can repair mismatches *in vitro* and triggers a DNA damage-induced G_2 checkpoint). However, unlike other eukaryotic MMR-deficient cells, the growth of the *Msh6*$^{-/-}$ and *Pms2*$^{-/-}$ DT40 B cells is greatly impaired. Moreover, they display abnormal morphology, most likely linked to spontaneous cell cycle alterations that include one round of endore-duplication. Based on the absence of a substantial increase in apoptosis and on the abnormal nuclear morphology, we posit that the 8n MMR-deficient DT40 cells undergo mitotic catastrophe (68). This unexpected phenotype contrasts with the viability of *Msh6*$^{-/-}$ and *Pms2*$^{-/-}$ mice (43,69) and with the fact that MSH2-, MSH3- or MSH6-deficient mouse B cells proliferate normally when stimulated *in vitro* (50,70,71). Nonetheless, germinal centre B lymphocytes in *Msh2*$^{-/-}$ mice show unusually high levels of genomic instability and compromised germinal centre reaction (66,71,72). Germinal centre B cells express low levels of p53 (73), which may distinguish them from *in vitro* activated B cells. That p53 may be implicated in this process is underscored by the finding that p53$^{-/-}$ *Msh2*$^{-/-}$ mouse embryo fibroblasts accumulate cells with 8n DNA content after genotoxic damage, which implies that MMR status and G_1 checkpoint abrogation affect ploidy control (74). Given that DT40 cells do not express p53, and thus that their G_1 checkpoint is compromised (75), they may be predisposed to re-replication (76), and this phenotype might be aggravated by the relaxation of the S (77) and G_2/M (15,54) checkpoints in MMR-deficient cells. Our results thus support a role for MMR in the prevention of re-replication in checkpoint-deficient DT40 cells.

MMR and *Ig* gene conversion

Although *Ig* GC is mediated by HR factors (33,35–37), MMR in vertebrate cells impairs this process when sequence heterology exceeds 1% (42–44,78). Accordingly, MSH6- or PMS2-deficient cells have a hyper-recombinogenic phenotype both in yeast and mammals (43,78). We demonstrate here that MMR is functional in DT40 cells (Figures 5 and 6). We, therefore, expected to find an effect of MMR deficiency on *Ig* GC. Surprisingly, we found MutSα and MutLα to be largely dispensable for *Ig* GC in DT40 cells. This does not mean they do not normally play a role during *Ig* GC resolution. Indeed, we detected a significant trend towards longer GC tracts, most notably in PMS2-deficient cells, which

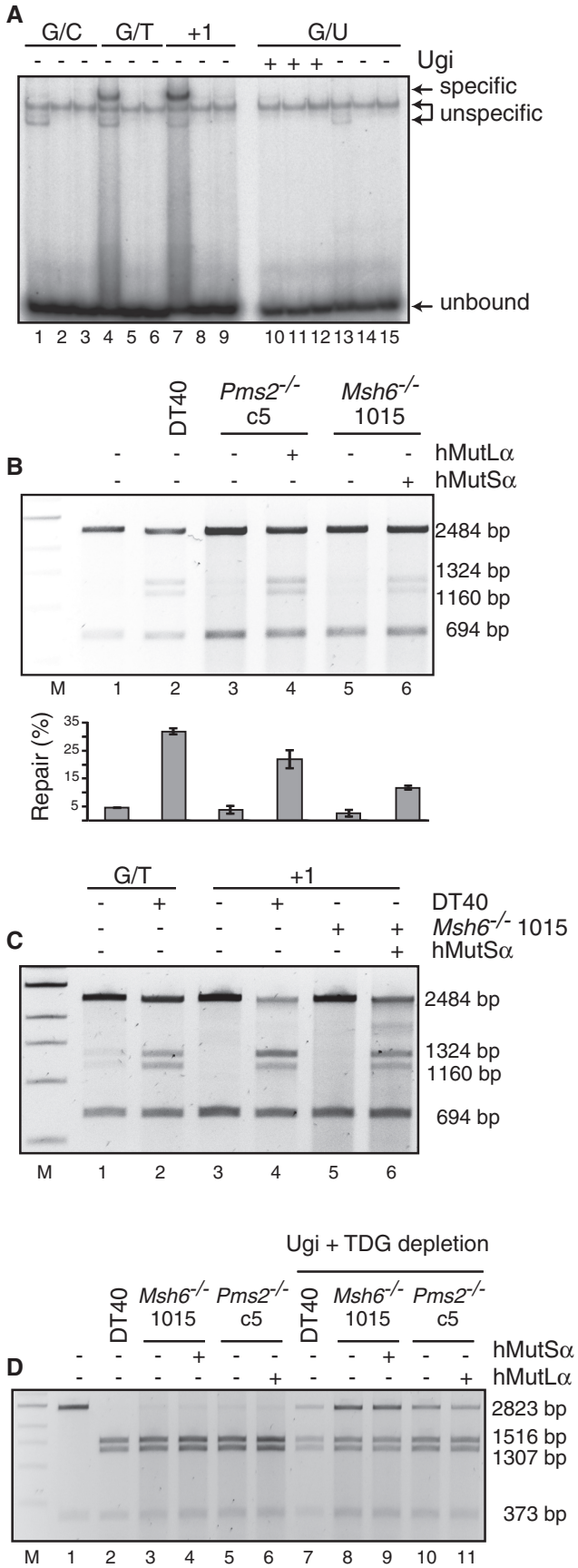

Figure 6. Mismatch binding and repair in DT40 cell extracts. (**A**) Gel-shift with DT40 WT cell extracts (lanes 1, 4, 7, 10 and 13), cell extracts of the *Msh6*$^{-/-}$ clones 1015 (lanes 2, 5, 8, 11 and 14) and 1c1 (lanes 3, 6, 9, 12 and 15). The extracts were incubated with the indicated substrates for 20 min at RT, run on a 5% TAE–polyacrylamide gel and exposed to a PhosphorImager screen. (**B**) MMR assays with extracts of DT40 WT, *Pms2*$^{-/-}$ and *Msh6*$^{-/-}$ cell lines. The extracts were incubated with a plasmid containing a G/T mismatch in a SalI restriction site and a nick in the T strand 350 nt 3′ from the mismatch. On repair of the mispaired T, the SalI restriction site is restored, and digestion with this enzyme gives rise to the 1324- and 1160-bp fragments in repair-proficient samples. The mean intensity + standard error proportion of these two product fragments over total signal from two experiments was quantified using ImageQuant and is plotted for each line below the gel. (**C**) Mismatch repair assay performed as in (B). Extracts of DT40 WT and *Msh6*$^{-/-}$ cells were incubated with a substrate containing a single-nucleotide insertion (+1). The G/T substrate served as a control of repair efficiency. (**D**) Mismatch repair assay carried out as described in (B) (lanes 2–6) or after immunodepletion of TDG and inhibition of UNG by the addition of Ugi (lanes 7–11). The substrate used in this assay contained a G/U mismatch in an AclI site and a nick in the U strand 350 nt 3′ from the mismatch. Repair of G/U to G/C restores the AclI site, and digestion with this enzyme gives rise to the 1516- and 1307-bp fragments in repair-proficient samples.

confirms that MMR affects resolution of the heteroduplex intermediates arising during *Ig* GC (46,47,79). But as *Ig* GC can still proceed at near normal frequency in the absence of MMR, there must be alternative ways to resolve the GC. On the other hand, as *Ig* GC involves synapses between donor ψV and acceptor *IgVλ* sequences that are 3 to >10% divergent (3), we expected to see its frequency increased in *Msh6*$^{-/-}$ and/or *Pms2*$^{-/-}$ cells. Yet, this was not apparent in the fluctuation analyses, despite the caveat imposed by the cell growth defects of the MMR-deficient cells. Moreover, evidence of *Ig* GC should have been seen by sequencing the *IgV* as additional conversion events other than the one correcting the single nucleotide frameshift, but this was also not the case. In addition, *Ig* GC generally prefers to use as donor the ψV most similar to the *IgV* (3,27), which implies that the HR pathway for *Ig* GC senses homology. As in WT cells, the most frequently used donor pseudogene in *Msh6*$^{-/-}$ and *Pms2*$^{-/-}$ DT40 cells was ψV8, which is the closest sequence homologue to DT40 *IgVλ*. This suggests that the MMR defect in these cells did not bring about a relaxation in *Ig* GC stringency. MutSβ could compensate for the lack of MutSα, given that it has been shown to contribute to repressing recombination between divergent sequences in yeast (80). However, MutSα has a much more prominent role than MutSβ in preventing recombination in mammalian cells (43), which, combined with our findings that MSH6-deficient DT40 extracts lack the ability to correct +1 loops, make this scenario unlikely. Similarly, although MutLα prevents homeologous recombination in yeast (78), its absence is unlikely to be compensated for by MutLγ (81), despite the fact that the latter factor is involved in recombination control in mammalian cells (53). Another scenario whereby MSH6- or MMR-deficiency would not affect *Ig* GC frequency would be if HR in DT40 cells were less sensitive to MMR and more permissive to heterology. However, this was also not the case, as <1% heterology dramatically reduced gene targeting efficiency in these cells. That this

was because MMR could not be formally demonstrated owing to the technical limitations caused by the deleterious effect of MMR deficiency on clonal expansion of DT40 cells. However, as anti-recombination is an evolutionary conserved function of MMR (44,58–61) and we show that MMR is active in DT40 cells, it is likely that it controls HR in birds. HR, but not *Ig* GC, being sensitive to heterologies in DT40, our results indicate a key difference between the pathways leading to gene targeting and *Ig* GC.

Why is the MMR system not involved in *Ig* GC in DT40 cells, when it controls HR and when it triggers SHM and CSR in mammalian cells? Our data suggest that part of the explanation might lie in the processing of AID-generated G/U mispairs. Purified human MutSα binds to G/U mispairs, albeit weaker than to G/T (63,82,83). We failed to detect a specific gel-shift with the G/U substrates in DT40 cell extracts, even though G/T and +1 substrates were bound efficiently (Figure 6A). This could mean either that chicken MutSα does not recognize G/U, or that the uracil was removed by glycosylases other than UNG present in the extracts, given that addition of Ugi had no effect. In an *in vitro* MMR assay, the G/U substrate was repaired extremely efficiently, and Ugi addition combined with TDG depletion brought about only a small reduction in efficiency, but this decrease was similar in MMR-proficient and MMR-deficient extracts. We, therefore, posit that the MMR system does not address G/U mispairs in DT40 extracts, possibly because of being outcompeted by BER factors. Should a similar situation prevail also *in vivo*, then it would explain why AID-induced G/U mispairs fail to trigger *Ig* GC in UNG-deficient, MMR-proficient cells (38,39). Still, this finding does not explain why MMR status does not affect *Ig* GC outcome in DT40 cells. It is possible that this is related to the recombinogenic phenotype of DT40 cells; as MMR is required to help maintain their genomic stability, MutSα and MutLα enzymes might be sequestered by HR in these cells *in vivo* and, therefore, unavailable to deal with GC events. Alternatively, the difference in sensitivity to heterology during gene targeting and *Ig* GC may indicate that the two processes proceed through different HR branches in DT40 cells. Our findings suggest that the *Ig* GC process in DT40 cells may represent a rare example of MMR-insensitive homeologous recombination.

SUPPLEMENTARY DATA

Supplementary Data are available at NAR Online: Supplementary Figures 1–6.

ACKNOWLEDGEMENTS

The authors are indebted to Michael Neuberger for discussions and support when the project was initiated at the MRC Laboratory of Molecular Biology, Cambridge, UK. They thank Jean-Marie Buerstedde, Hiroshi Arakawa, Katja Kratz, Stephanie Bergeron and Mariela Artola for reagents; Julian Sale and Anja Bielinsky for critical reading of the manuscript; and Tiago Chiavegatti for advice on statistics and Astrid Zahn for technical help.

FUNDING

Canadian Institutes of Health Research [MOP84543 to J.M.D.N.]; Canada Research Chair tier 2 (to J.M.D.N.). Michel Saucier fellowship through the Department of Microbiology and Immunology, Université de Montréal (to V.A.C. in part); Swiss National Science Foundation [310030A-118158 to J.J.]. Funding for open access charge: Institutional funds (to J.M.D.N.).

Conflict of interest statement. None declared.

REFERENCES

1. Di Noia,J.M. and Neuberger,M.S. (2007) Molecular mechanisms of antibody somatic hypermutation. *Annu. Rev. Biochem.*, **76**, 1–22.
2. Peled,J.U., Kuang,F.L., Iglesias-Ussel,M.D., Roa,S., Kalis,S.L., Goodman,M.F. and Scharff,M.D. (2008) The biochemistry of somatic hypermutation. *Annu. Rev. Immunol.*, **26**, 481–511.
3. Reynaud,C.A., Anquez,V., Grimal,H. and Weill,J.C. (1987) A hyperconversion mechanism generates the chicken light chain preimmune repertoire. *Cell*, **48**, 379–388.
4. Reynaud,C.A., Dahan,A., Anquez,V. and Weill,J.C. (1989) Somatic hyperconversion diversifies the single Vh gene of the chicken with a high incidence in the D region. *Cell*, **59**, 171–183.
5. Chaudhuri,J. and Alt,F.W. (2004) Class-switch recombination: interplay of transcription, DNA deamination and DNA repair. *Nat. Rev. Immunol.*, **4**, 541–552.
6. Stavnezer,J., Guikema,J.E.J. and Schrader,C.E. (2008) Mechanism and regulation of class switch recombination. *Annu. Rev. Immunol.*, **26**, 261–292.
7. Arakawa,H., Hauschild,J. and Buerstedde,J.M. (2002) Requirement of the activation-induced deaminase (AID) gene for immunoglobulin gene conversion. *Science*, **295**, 1301–1306.
8. Harris,R.S., Sale,J.E., Petersen-Mahrt,S.K. and Neuberger,M.S. (2002) AID is essential for immunoglobulin V gene conversion in a cultured B cell line. *Curr. Biol.*, **12**, 435–438.
9. Muramatsu,M., Kinoshita,K., Fagarasan,S., Yamada,S., Shinkai,Y. and Honjo,T. (2000) Class switch recombination and hypermutation require activation-induced cytidine deaminase (AID), a potential RNA editing enzyme. *Cell*, **102**, 553–563.
10. Di Noia,J. and Neuberger,M.S. (2002) Altering the pathway of immunoglobulin hypermutation by inhibiting uracil-DNA glycosylase. *Nature*, **419**, 43–48.
11. Rada,C., Di Noia,J.M. and Neuberger,M.S. (2004) Mismatch recognition and uracil excision provide complementary paths to both Ig switching and the A/T-focused phase of somatic mutation. *Mol. Cell*, **16**, 163–171.
12. Rada,C., Williams,G.T., Nilsen,H., Barnes,D.E., Lindahl,T. and Neuberger,M.S. (2002) Immunoglobulin isotype switching is inhibited and somatic hypermutation perturbed in UNG-deficient mice. *Curr. Biol.*, **12**, 1748–1755.
13. Di Noia,J.M., Williams,G.T., Chan,D.T.Y., Buerstedde,J.-M., Baldwin,G.S. and Neuberger,M.S. (2007) Dependence of antibody gene diversification on uracil excision. *J. Exp. Med.*, **204**, 3209–3219.
14. Rada,C., Ehrenstein,M.R., Neuberger,M.S. and Milstein,C. (1998) Hot spot focusing of somatic hypermutation in MSH2-deficient mice suggests two stages of mutational targeting. *Immunity*, **9**, 135–141.
15. Jiricny,J. (2006) The multifaceted mismatch-repair system. *Nat. Rev. Mol. Cell. Biol.*, **7**, 335–346.
16. Kunkel,T.A. and Erie,D.A. (2005) DNA mismatch repair. *Annu. Rev. Biochem.*, **74**, 681–710.
17. Stavnezer,J. and Schrader,C.E. (2006) Mismatch repair converts AID-instigated nicks to double-strand breaks for antibody class-switch recombination. *Trends Genet.*, **22**, 23–28.

18. Bardwell,P.D., Woo,C.J., Wei,K., Li,Z., Martin,A., Sack,S.Z., Parris,T., Edelmann,W. and Scharff,M.D. (2004) Altered somatic hypermutation and reduced class-switch recombination in exonuclease 1-mutant mice. *Nat. Immunol.*, **5**, 224–229.
19. Delbos,F., Aoufouchi,S., Faili,A., Weill,J.C. and Reynaud,C.A. (2007) DNA polymerase eta is the sole contributor of A/T modifications during immunoglobulin gene hypermutation in the mouse. *J. Exp. Med.*, **204**, 17–23.
20. Zeng,X., Winter,D.B., Kasmer,C., Kraemer,K.H., Lehmann,A.R. and Gearhart,P.J. (2001) DNA polymerase eta is an A-T mutator in somatic hypermutation of immunoglobulin variable genes. *Nat. Immunol.*, **2**, 537–541.
21. Langerak,P., Nygren,A.O., Krijger,P.H., van den Berk,P.C. and Jacobs,H. (2007) A/T mutagenesis in hypermutated immunoglobulin genes strongly depends on PCNAK164 modification. *J. Exp. Med.*, **204**, 1989–1998.
22. Roa,S., Avdievich,E., Peled,J.U., Maccarthy,T., Werling,U., Kuang,F.L., Kan,R., Zhao,C., Bergman,A., Cohen,P.E. *et al.* (2008) Ubiquitylated PCNA plays a role in somatic hypermutation and class-switch recombination and is required for meiotic progression. *Proc. Natl. Acad. Sci. USA*, **105**, 16248–16253.
23. Ehrenstein,M.R., Rada,C., Jones,A.M., Milstein,C. and Neuberger,M.S. (2001) Switch junction sequences in PMS2-deficient mice reveal a microhomology-mediated mechanism of Ig class switch recombination. *Proc. Natl. Acad. Sci. USA*, **98**, 14553–14558.
24. Shen,H.M., Tanaka,A., Bozek,G., Nicolae,D. and Storb,U. (2006) Somatic hypermutation and class switch recombination in Msh6(−/−)Ung(−/−) double-knockout mice. *J. Immunol.*, **177**, 5386–5392.
25. Arakawa,H. and Buerstedde,J.-M. (2004) Immunoglobulin gene conversion: insights from bursal B cells and the DT40 cell line. *Dev. Dyn.*, **229**, 458–464.
26. Weinstein,P.D., Anderson,A.O. and Mage,R.G. (1994) Rabbit IgH sequences in appendix germinal centers: VH diversification by gene conversion-like and hypermutation mechanisms. *Immunity*, **1**, 647–659.
27. McCormack,W.T. and Thompson,C.B. (1990) Chicken IgL variable region gene conversions display pseudogene donor preference and 5' to 3' polarity. *Genes Dev.*, **4**, 548–558.
28. Buerstedde,J.M., Reynaud,C.A., Humphries,E.H., Olson,W., Ewert,D.L. and Weill,J.C. (1990) Light chain gene conversion continues at high rate in an ALV-induced cell line. *EMBO J.*, **9**, 921–927.
29. Kim,S., Humphries,E.H., Tjoelker,L., Carlson,L. and Thompson,C.B. (1990) Ongoing diversification of the rearranged immunoglobulin light-chain gene in a bursal lymphoma cell line. *Mol. Cell. Biol.*, **10**, 3224–3231.
30. Arakawa,H. and Buerstedde,J.M. (2009) Activation-induced cytidine deaminase-mediated hypermutation in the DT40 cell line. *Philos. Trans. R Soc. Lond. B Biol. Sci.*, **364**, 639–644.
31. Tang,E.S. and Martin,A. (2007) Immunoglobulin gene conversion: Synthesizing antibody diversification and DNA repair. *DNA Repair (Amst)*, **6**, 1557–1571.
32. Sonoda,E., Morrison,C., Yamashita,Y.M., Takata,M. and Takeda,S. (2001) Reverse genetic studies of homologous DNA recombination using the chicken B-lymphocyte line, DT40. *Philos. Trans. R Soc. Lond. B Biol. Sci.*, **356**, 111–117.
33. Sale,J.E. (2004) Immunoglobulin diversification in DT40: a model for vertebrate DNA damage tolerance. *DNA Repair (Amst)*, **3**, 693–702.
34. Sale,J.E., Calandrini,D.M., Takata,M., Takeda,S. and Neuberger,M.S. (2001) Ablation of XRCC2/3 transforms immunoglobulin V gene conversion into somatic hypermutation. *Nature*, **412**, 921–926.
35. Longerich,S., Orelli,B.J., Martin,R.W., Bishop,D.K. and Storb,U. (2008) Brca1 in immunoglobulin gene conversion and somatic hypermutation. *DNA Repair (Amst)*, **7**, 253–266.
36. Hatanaka,A., Yamazoe,M., Sale,J.E., Takata,M., Yamamoto,K., Kitao,H., Sonoda,E., Kikuchi,K., Yonetani,Y. and Takeda,S. (2005) Similar effects of Brca2 truncation and Rad51 paralog deficiency on immunoglobulin V gene diversification in DT40 cells support an early role for Rad51 paralogs in homologous recombination. *Mol. Cell. Biol.*, **25**, 1124–1134.
37. Bezzubova,O., Silbergleit,A., Yamaguchi-Iwai,Y., Takeda,S. and Buerstedde,J.-M. (1997) Reduced X-ray resistance and homologous recombination frequencies in a RAD54−/− mutant of the chicken DT40 cell line. *Cell*, **89**, 185–193.
38. Di Noia,J.M. and Neuberger,M.S. (2004) Immunoglobulin gene conversion in chicken DT40 cells largely proceeds through an abasic site intermediate generated by excision of the uracil produced by AID-mediated deoxycytidine deamination. *Eur. J. Immunol.*, **34**, 504–508.
39. Saribasak,H., Saribasak,N.N., Ipek,F.M., Ellwart,J.W., Arakawa,H. and Buerstedde,J.M. (2006) Uracil DNA glycosylase disruption blocks Ig gene conversion and induces transition mutations. *J. Immunol.*, **176**, 365–371.
40. Roa,S., Li,Z., Peled,J.U., Zhao,C., Edelmann,W. and Scharff,M.D. (2010) MSH2/MSH6 complex promotes error-free repair of AID-induced dU:G mispairs as well as error-prone hypermutation of A:T sites. *PLoS One*, **5**, e11182.
41. Abuin,A., Zhang,H. and Bradley,A. (2000) Genetic analysis of mouse embryonic stem cells bearing Msh3 and Msh2 single and compound mutations. *Mol. Cell. Biol.*, **20**, 149–157.
42. de Wind,N., Dekker,M., Berns,A., Radman,M. and te Riele,H. (1995) Inactivation of the mouse Msh2 gene results in mismatch repair deficiency, methylation tolerance, hyperrecombination, and predisposition to cancer. *Cell*, **82**, 321–330.
43. de Wind,N., Dekker,M., Claij,N., Jansen,L., van Klink,Y., Radman,M., Riggins,G., van der Valk,M., van't Wout,K. and te Riele,H. (1999) HNPCC-like cancer predisposition in mice through simultaneous loss of Msh3 and Msh6 mismatch-repair protein functions. *Nat. Genet.*, **23**, 359–362.
44. Elliott,B. and Jasin,M. (2001) Repair of double-strand breaks by homologous recombination in mismatch repair-defective mammalian cells. *Mol. Cell. Biol.*, **21**, 2671–2682.
45. Evans,E. and Alani,E. (2000) Roles for mismatch repair factors in regulating genetic recombination. *Mol. Cell. Biol.*, **20**, 7839–7844.
46. Chen,J.-M., Cooper,D.N., Chuzhanova,N., Férec,C. and Patrinos,G.P. (2007) Gene conversion: mechanisms, evolution and human disease. *Nat. Rev. Genet.*, **8**, 762–775.
47. Haber,J.E., Ira,G., Malkova,A. and Sugawara,N. (2004) Repairing a double-strand chromosome break by homologous recombination: revisiting Robin Holliday's model. *Philos. Trans. R Soc. Lond. B Biol. Sci.*, **359**, 79–86.
48. Arakawa,H., Lodygin,D. and Buerstedde,J.M. (2001) Mutant loxP vectors for selectable marker recycle and conditional knock-outs. *BMC Biotechnol.*, **1**, 7.
49. Fischer,F., Baerenfaller,K. and Jiricny,J. (2007) 5-Fluorouracil is efficiently removed from DNA by the base excision and mismatch repair systems. *Gastroenterology*, **133**, 1858–1868.
50. Li,Z., Scherer,S.J., Ronai,D., Iglesias-Ussel,M.D., Peled,J.U., Bardwell,P.D., Zhuang,M., Lee,K., Martin,A., Edelmann,W. *et al.* (2004) Examination of Msh6- and Msh3-deficient mice in class switching reveals overlapping and distinct roles of MutS homologues in antibody diversification. *J. Exp. Med.*, **200**, 47–59.
51. Martomo,S.A., Yang,W.W. and Gearhart,P.J. (2004) A role for Msh6 but not Msh3 in somatic hypermutation and class switch recombination. *J. Exp. Med.*, **200**, 61–68.
52. Wiesendanger,M., Kneitz,B., Edelmann,W. and Scharff,M.D. (2000) Somatic hypermutation in MutS homologue (MSH)3-, MSH6-, and MSH3/MSH6-deficient mice reveals a role for the MSH2-MSH6 heterodimer in modulating the base substitution pattern. *J. Exp. Med.*, **191**, 579–584.
53. Lipkin,S.M., Wang,V., Jacoby,R., Banerjee-Basu,S., Baxevanis,A.D., Lynch,H.T., Elliott,R.M. and Collins,F.S. (2000) MLH3: a DNA mismatch repair gene associated with mammalian microsatellite instability. *Nat. Genet.*, **24**, 27–35.
54. Hawn,M.T., Umar,A., Carethers,J.M., Marra,G., Kunkel,T.A., Boland,C.R. and Koi,M. (1995) Evidence for a connection between the mismatch repair system and the G2 cell cycle checkpoint. *Cancer Res.*, **55**, 3721–3725.
55. Seo,H., Masuoka,M., Murofushi,H., Takeda,S., Shibata,T. and Ohta,K. (2005) Rapid generation of specific antibodies by enhanced homologous recombination. *Nat. Biotechnol.*, **23**, 731–735.
56. Nelson,J.A., Carpenter,J.W., Rose,L.M. and Adamson,D.J. (1975) Mechanisms of action of 6-thioguanine, 6-mercaptopurine, and 8-azaguanine. *Cancer Res.*, **35**, 2872–2878.

57. Buerstedde,J.M. and Takeda,S. (1991) Increased ratio of targeted to random integration after transfection of chicken B cell lines. *Cell*, **67**, 179–188.
58. Worth,L., Clark,S., Radman,M. and Modrich,P. (1994) Mismatch repair proteins MutS and MutL inhibit RecA-catalyzed strand transfer between diverged DNAs. *Proc. Natl. Acad. Sci. USA*, **91**, 3238–3241.
59. Selva,E.M., New,L., Crouse,G.F. and Lahue,R.S. (1995) Mismatch correction acts as a barrier to homeologous recombination in Saccharomyces cerevisiae. *Genetics*, **139**, 1175–1188.
60. Elliott,B., Richardson,C., Winderbaum,J., Nickoloff,J.A. and Jasin,M. (1998) Gene conversion tracts from double-strand break repair in mammalian cells. *Mol. Cell. Biol.*, **18**, 93–101.
61. te Riele,H., Maandag,E.R. and Berns,A. (1992) Highly efficient gene targeting in embryonic stem cells through homologous recombination with isogenic DNA constructs. *Proc. Natl. Acad. Sci. USA*, **89**, 5128–5132.
62. Jiricny,J., Hughes,M., Corman,N. and Rudkin,B.B. (1988) A human 200-kDa protein binds selectively to DNA fragments containing G.T mismatches. *Proc. Natl. Acad. Sci. USA*, **85**, 8860–8864.
63. Hughes,M.J. and Jiricny,J. (1992) The purification of a human mismatch-binding protein and identification of its associated ATPase and helicase activities. *J. Biol. Chem.*, **267**, 23876–23882.
64. Hendrich,B., Hardeland,U., Ng,H.H., Jiricny,J. and Bird,A. (1999) The thymine glycosylase MBD4 can bind to the product of deamination at methylated CpG sites. *Nature*, **401**, 301–304.
65. Di Noia,J.M., Rada,C. and Neuberger,M.S. (2006) SMUG1 is able to excise uracil from immunoglobulin genes: insight into mutation versus repair. *EMBO J.*, **25**, 585–595.
66. Frey,S., Bertocci,B., Delbos,F., Quint,L., Weill,J.C. and Reynaud,C.A. (1998) Mismatch repair deficiency interferes with the accumulation of mutations in chronically stimulated B cells and not with the hypermutation process. *Immunity*, **9**, 127–134.
67. Schrader,C.E., Edelmann,W., Kucherlapati,R. and Stavnezer,J. (1999) Reduced isotype switching in splenic B cells from mice deficient in mismatch repair enzymes. *J. Exp. Med.*, **190**, 323–330.
68. Vitale,I., Galluzzi,L., Castedo,M. and Kroemer,G. (2011) Mitotic catastrophe: a mechanism for avoiding genomic instability. *Nat. Rev. Mol. Cell. Biol.*, **12**, 385–392.
69. Baker,S.M., Bronner,C.E., Zhang,L., Plug,A.W., Robatzek,M., Warren,G., Elliott,E.A., Yu,J., Ashley,T., Arnheim,N. *et al.* (1995) Male mice defective in the DNA mismatch repair gene PMS2 exhibit abnormal chromosome synapsis in meiosis. *Cell*, **82**, 309–319.
70. Kim,N. and Storb,U. (1998) The role of DNA repair in somatic hypermutation of immunoglobulin genes. *J. Exp. Med.*, **187**, 1729–1733.
71. Vora,K.A., Tumas-Brundage,K.M., Lentz,V.M., Cranston,A., Fishel,R. and Manser,T. (1999) Severe attenuation of the B cell immune response in Msh2-deficient mice. *J. Exp. Med.*, **189**, 471–482.
72. Alabyev,B. and Manser,T. (2002) Bcl-2 rescues the germinal center response but does not alter the V gene somatic hypermutation spectrum in MSH2-deficient mice. *J. Immunol.*, **169**, 3819–3824.
73. Phan,R.T. and Dalla-Favera,R. (2004) The BCL6 proto-oncogene suppresses p53 expression in germinal-centre B cells. *Nature*, **432**, 635–639.
74. Strathdee,G., Sansom,O.J., Sim,A., Clarke,A.R. and Brown,R. (2001) A role for mismatch repair in control of DNA ploidy following DNA damage. *Oncogene*, **20**, 1923–1927.
75. Takao,N., Kato,H., Mori,R., Morrison,C., Sonoda,E., Sun,X., Shimizu,H., Yoshioka,K.-i., Takeda,S. and Yamamoto,K. (1999) Disruption of ATM in p53-null cells causes multiple functional abnormalities in cellular response to ionizing radiation. *Oncogene*, **18**, 7002–7009.
76. Vaziri,C., Saxena,S., Jeon,Y., Lee,C., Murata,K., Machida,Y., Wagle,N., Hwang,D.S. and Dutta,A. (2003) A p53-dependent checkpoint pathway prevents rereplication. *Mol. Cell*, **11**, 997–1008.
77. Brown,K.D., Rathi,A., Kamath,R., Beardsley,D.I., Zhan,Q., Mannino,J.L. and Baskaran,R. (2003) The mismatch repair system is required for S-phase checkpoint activation. *Nat. Genet.*, **33**, 80–84.
78. Erdeniz,N., Nguyen,M., Deschênes,S.M. and Liskay,R.M. (2007) Mutations affecting a putative MutLalpha endonuclease motif impact multiple mismatch repair functions. *DNA Repair*, **6**, 1463–1470.
79. Bollag,R.J., Elwood,D.R., Tobin,E.D., Godwin,A.R. and Liskay,R.M. (1992) Formation of heteroduplex DNA during mammalian intrachromosomal gene conversion. *Mol. Cell. Biol.*, **12**, 1546–1552.
80. Nicholson,A., Hendrix,M., Jinks-Robertson,S. and Crouse,G.F. (2000) Regulation of mitotic homeologous recombination in yeast. Functions of mismatch repair and nucleotide excision repair genes. *Genetics*, **154**, 133–146.
81. Cannavo,E., Marra,G., Sabates-Bellver,J., Menigatti,M., Lipkin,S.M., Fischer,F., Cejka,P. and Jiricny,J. (2005) Expression of the MutL homologue hMLH3 in human cells and its role in DNA mismatch repair. *Cancer Res.*, **65**, 10759–10766.
82. Warren,J.J., Pohlhaus,T.J., Changela,A., Iyer,R.R., Modrich,P.L. and Beese,L.S. (2007) Structure of the human MutSalpha DNA lesion recognition complex. *Mol. Cell*, **26**, 579–592.
83. Wilson,T.M., Vaisman,A., Martomo,S.A., Sullivan,P., Lan,L., Hanaoka,F., Yasui,A., Woodgate,R. and Gearhart,P.J. (2005) MSH2-MSH6 stimulates DNA polymerase eta, suggesting a role for A:T mutations in antibody genes. *J. Exp. Med.*, **201**, 637–645.